





Title	Electromagnetically induced transparency from first-order dynamical systems
Authors	Clementi, Marco;Galli, Matteo;O'Faolain, Liam;Gerace, Dario
Publication date	2021-11-30
Original Citation	Clementi, M., Galli, M., O'Faolain, L. and Gerace, D. (2021) 'Electromagnetically induced transparency from first-order dynamical systems', Physical Review B, 104(20), 205434 (12pp). doi: 10.1103/PhysRevB.104.205434
Type of publication	Article (peer-reviewed)
Link to publisher's version	10.1103/PhysRevB.104.205434
Rights	© 2021, American Physical Society. All rights reserved.
Download date	2024-05-14 00:53:12
Item downloaded from	https://hdl.handle.net/10468/12476

Electromagnetically induced transparency from first-order dynamical systems

Marco Clementi ¹, Matteo Galli ¹, Liam O'Faolain ^{2,3} and Dario Gerace ^{1,*}

¹*Dipartimento di Fisica, Università degli Studi di Pavia, Via Agostino Bassi 6, I-27100 Pavia, Italy*

²*Centre for Advanced Photonics and Process Analysis, Munster Technological University, Rossa Ave Bishopstown, Cork T12 P928, Ireland*

³*Photonics, Tyndall National Institute, Lee Maltings Complex Dyke Parade, Cork T12 R5CP, Ireland*



(Received 13 July 2021; accepted 11 November 2021; published 30 November 2021)

We show how a strongly driven single-mode oscillator coupled to a first-order dynamical system gives rise to induced absorption or gain of a weak probe beam and associated fast or slow light depending on the detuning conditions. We derive the analytic solutions to the dynamic equations of motion, showing that the electromagnetically induced transparency- (EIT-) like response is a general phenomenology, potentially occurring in any nonlinear oscillator coupled to first-order dynamical systems. The resulting group delay (or advance) of the probe is fundamentally determined by the system damping rate. To illustrate the practical impact of this general theoretical framework, we quantitatively assess the observable consequences of either thermo-optic or free-carrier dispersion effects in conventional semiconductor microcavities in control/probe experiments, highlighting the generality of this physical mechanism and its potential for the realization of EIT-like phenomena in integrated and cost-effective photonic devices.

DOI: [10.1103/PhysRevB.104.205434](https://doi.org/10.1103/PhysRevB.104.205434)

I. INTRODUCTION

Electromagnetically induced transparency (EIT) [1] and its analogs [2] gathered high interest over the past few decades. In its broadest definition, the phenomenon consists of the appearance of a narrow transmission window in an otherwise absorptive medium, such as an atomic cloud or a solid-state medium. This is typically associated with a steep normal dispersion, owing to the analytic relation between the real and the imaginary parts of the dielectric response function, which gives rise to large group delays (slow light) for light pulses within the induced transparency spectral window [3] with applications ranging from optical delay lines to photonic quantum memories [4].

After the first experimental evidence shown on atomic clouds [5], and the subsequent demonstration of slowing light down to 17 m/s in an ultracold gas [6], several EIT analogs have been reported in solid-state systems, such as semiconductor quantum dots [7,8], coupled resonators [9], metamaterials [10], cavity optomechanics [11,12], and acousto-optic resonators [13,14] with group delays or advances as high as a few microseconds. The possibility to achieve optical delay was specifically investigated in integrated photonics due to the interest for the implementation of small-footprint delay lines with applications ranging from optical memories [15] to quantum computing [16].

All the EIT analogs quoted above share a common feature: the electromagnetic field coherently interacts with a physical system displaying a second-order dynamic response, characteristic of harmonic oscillators. This may be either a Λ -type three-level system in the case of conventional EIT [1] or a

mechanical harmonic oscillator in the case of optomechanically induced transparency [11,12,17] or again an acoustic mode of the structure in the case of Brillouin scattering induced transparency [13,14]. Intuitively, all these examples have in common the coherent exchange of energy between the field and the harmonic degree of freedom, which results in the emergence of the induced transparency window and the associated slow or fast light effects [12].

In contrast, little effort has been devoted so far to investigate the interaction between the electromagnetic field and a first-order (i.e., dissipative) system. In this paper, we present a theoretical model of a generic single-mode oscillator driven by an intense control and a weak probe field and nonlinearly coupled to a first-order dynamical system. We show how this very general physical configuration gives rise to an EIT-analog response. In light of the several possible physical realizations of this model, our approach represents a novel framework to investigate EIT and its peculiar consequences on light dispersion in various and unconventional experimental settings. In particular, we first show that any dynamical quantity characterized by a decay rate γ and mediating an effective Kerr-type nonlinear interaction on the localized electromagnetic field gives rise to a spectral hole or antihole. These can be experimentally evidenced by a weak probe superimposed to an intense control beam, associated group advance, or delay, respectively.

We then show how this phenomenology stems from two paradigmatic examples of effective nonlinearities in semiconductor resonators: the first-order dynamical response associated with the thermo-optic (TO) effect, and the one due to free-carrier dispersion. As a consequence, any resonator realized in material platforms subject to such types of nonlinear behavior can be potentially engineered to display an EIT-like response and to exploit their observable consequences,

*dario.gerace@unipv.it

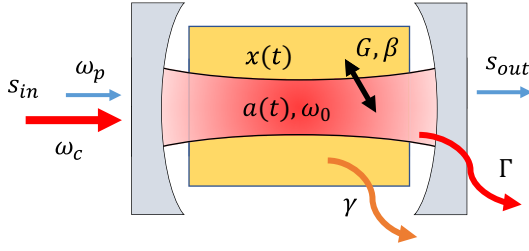


FIG. 1. Scheme of the physical system under analysis. An optical resonator, characterized by an intracavity field amplitude $a(t)$, bare resonance frequency ω_0 , and intrinsic decay rate Γ , is coherently driven by a control (red arrow) and a probe (blue arrow) input fields. The confined mode is coupled to a first-order system (yellow), uniquely characterized by a dynamical variable $x(t)$ and an incoherent dissipation rate γ through the coupling parameters G and β .

i.e., large group delays or advances. We note that, whereas the first experimental evidences for thermo-optically induced transparency have already been reported [18,19], the free-carrier induced transparency phenomenon predicted here has not been observed, nor theoretically described, up to date. Although this paper aims at providing a theoretical framework for the formulation and interpretation of a general class of phenomena, our purpose is also to introduce the key analytic tools to design the practical implementation of large group delays and advances in actual photonic devices based on conventional material platforms, thus, fostering future experiments allowing to leverage the stringent requirements of typical EIT-analog physics.

The paper is organized as follows. In Sec. II we show how EIT can emerge from the interaction between a confined optical mode and a first-order system within a general theoretical framework. First, we present the relevant equations of motion, their steady-state solutions (Sec. II A), and a linearized solution assuming a control-probe excitation (Sec. II B). In Sec. III, we predict how this phenomenon can be observed in actual state-of-art semiconductor microcavities, mediated either by the thermo-optic effect (Sec. III A) or by the free-carrier dispersion effect (Sec. III B), and we finally provide a comparison of the relevant figures of merit (Sec. III C).

II. GENERAL MODEL

Consider a single-mode oscillator, which for simplicity might be thought of as an optical cavity (e.g., sketched in Fig. 1), characterized by a time-dependent classical field amplitude $a(t)$, a bare resonance frequency ω_0 a decay rate Γ , and driven by a forcing amplitude s_{in} . Next, let us consider a second physical system, described by a classical degree of freedom $x(t)$ and obeying the following first-order rate equation:

$$\frac{d}{dt}x(t) = \beta|a(t)|^2 - \gamma x(t), \quad (1)$$

where the forcing term is proportional to the intracavity energy $|a(t)|^2$ through the absorptive parameter β , whereas the dissipation rate γ represents the intrinsic system damping (decay).

We will, henceforth, assume that the actual resonance frequency parametrically depends on $x(t)$ such that $\bar{\omega}_0 = \omega_0 + Gx(t)$ in which G is a coupling term and $\bar{\omega}_0$ is the resonance frequency in the presence of the nonlinear shift. We assume the field amplitude to obey the following dynamical equation:

$$\frac{d}{dt}a(t) = \left(i\omega_0 - \frac{\Gamma}{2}\right)a(t) + iGx(t)a(t) + \sqrt{\eta}\Gamma s_{in}(t), \quad (2)$$

in which η represents the in-coupling efficiency to the single-mode oscillator such that the in-coupling rate is given as $\Gamma_{in} = \eta\Gamma$. The interaction term in Eq. (2) can be easily interpreted as a Kerr-type (i.e., intensity-dependent) shift of the cavity resonance frequency, typically observed in nonlinear optical resonators. However, in contrast with the instantaneous Kerr response, the timescale of such an interaction is here governed by the characteristic damping rate γ , typical of effective nonlinearities. In analogy with the usual phenomenology of the Kerr response, we will assume $G < 0$ for the moment, with straightforward generalization.

We will now study the dynamics of the system response first in the presence of a single driving field with a constant amplitude and then in a control-and-probe excitation configuration.

A. Steady-state solution: optical bistability

Consider a monochromatic driving field (henceforth, referred to as the “control field”) in the form

$$s_{in}(t) = \bar{s}_{in}e^{i\omega_c t}. \quad (3)$$

The steady-state solutions to Eqs. (1) and (2) are as follows:

$$\bar{a} = \frac{\sqrt{\eta}\Gamma}{i\bar{\Delta} + \Gamma/2}\bar{s}_{in}, \quad \bar{x} = \frac{\beta}{\gamma}|\bar{a}|^2, \quad (4)$$

where $\bar{\Delta} = \omega_c - \bar{\omega}_0 = \omega_c - \omega_0 - G\bar{x}$ is the detuning between input and intracavity field renormalized by the presence of a power-dependent shift and $|\bar{a}|^2$ represents the intracavity energy.

By analogy with the theory of optical bistability for a localized mode coupled to a Kerr medium [20], Eqs. (4) can be rewritten in the form

$$\frac{|\bar{a}|^2}{|\bar{s}_{in}|^2} = \frac{4\eta/\Gamma}{1 + (2\bar{\Delta}/\Gamma + |\bar{a}|^2/|\bar{a}_b|^2)^2}, \quad (5)$$

where we defined the characteristic bistability energy $|\bar{a}_b|^2 = -\gamma\Gamma/(2G\beta)$. The solution of Eq. (5) may exhibit a characteristic “sawtooth” lineshape as a function of the detuning $\bar{\Delta} = \omega_c - \omega_0$ and depending on $|\bar{a}|^2$ as shown in Fig. 2 and as already reported [21]. In fact, in the presence of a sufficiently intense driving field ($|\bar{a}|^2 \gg |\bar{a}_b|^2$) and appropriate detuning conditions ($\bar{\Delta} > \frac{\sqrt{3}}{2}\Gamma$) there are three possible solutions to the nonlinear equation, associated with two stable and one unstable equilibrium states, respectively [21,22]. In actual physical systems, the appropriate stable solution should be chosen according to the experimental conditions.

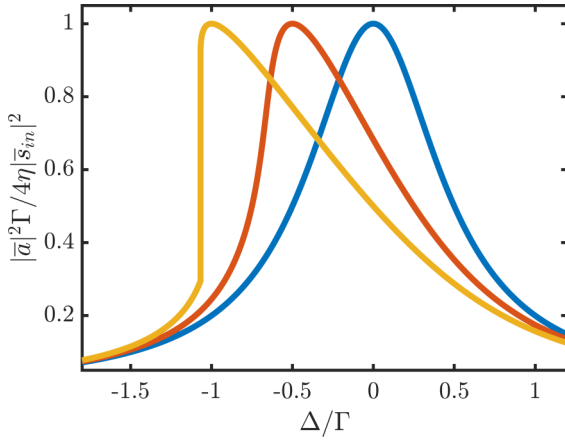


FIG. 2. Normalized intracavity energy as a function of the detuning between the control and the bare cavity frequencies $\Delta = \omega_c - \omega_0$ in the presence of a constant driving field \bar{s}_{in} . The increased coupled power (and, consequently, resonance shift) at lower detuning results in a characteristic sawtooth lineshape typical of bistable systems. The blue line represents the system response at low control power (peak cavity energy: $|\bar{a}|^2 = 10^{-3}|\bar{a}_b|^2$), the red (peak $|\bar{a}|^2 = |\bar{a}_b|^2$) and yellow (peak $|\bar{a}|^2 = 2|\bar{a}_b|^2$) curves represent the system response at increasing input power.

B. Dynamic solution: induced absorption and gain

1. Linearized dynamics

We will now investigate the system response in the presence of an intense control field in the form given in Eq. (3), and a weak “probe field” $\delta s_{in}(t) = s_p e^{i(\omega_c - \Omega)t}$ such that the overall driving term can be written as

$$s_{in}(t) = \bar{s}_{in} e^{i\omega_c t} + s_p e^{i(\omega_c - \Omega)t}, \quad (6)$$

where $|s_p|^2 \ll |\bar{s}_{in}|^2$. Note that the input intensity displays an optical beating occurring at the control-probe detuning frequency, Ω .

Under this assumption, we will model both the optical resonator and the first-order system responses as a steady state (i.e., mean-field) value, adding on top of it a small time-dependent perturbation,

$$a(t) = \bar{a} e^{i\omega_c t} + \delta a(t), \quad (7a)$$

$$x(t) = \bar{x} + \delta x(t). \quad (7b)$$

The weak probe field can then be included in the model by linearizing the dynamical Eqs. (1) and (2) at the equilibrium point, following a conventionally employed approach [11]. By inserting the dynamical variables defined in Eqs. (7) into the coupled differential equations we get

$$\frac{d}{dt} \delta a(t) = \left(i\bar{\omega}_0 - \frac{\Gamma}{2} \right) \delta a(t) + iG\bar{a} \delta x(t) + \sqrt{\eta}\Gamma \delta s_{in}(t), \quad (8a)$$

$$\frac{d}{dt} \delta x(t) = \beta [\bar{a}^* \delta a(t) + \bar{a} \delta a^*(t)] - \gamma \delta x(t). \quad (8b)$$

The solution can be found under the following ansatz:

$$\begin{aligned} \delta a(t) &= A_p^- e^{i(\omega_c - \Omega)t} + A_p^+ e^{i(\omega_c + \Omega)t}, \\ \delta x(t) &= X e^{-i\Omega t} + X^* e^{+i\Omega t}. \end{aligned}$$

After including the latter into Eqs. (8) and separating terms according to their time dependence, we finally derive the following expressions for the oscillation amplitudes:

$$A_p^- = \frac{iG\bar{a}X + \sqrt{\eta}\Gamma s_p}{i(\bar{\Delta} - \Omega) + \Gamma/2}, \quad (9a)$$

$$A_p^+ = \frac{iG\bar{a}}{i(\bar{\Delta} + \Omega) + \Gamma/2} X^*, \quad (9b)$$

$$X = \frac{\beta}{-i\Omega + \gamma} [\bar{a}^* A_p^- + \bar{a} (A_p^+)^*]. \quad (9c)$$

2. Analytic solution

The formal expressions given in Eqs. (9) can now be used to derive explicit analytic expressions for A_p^- , A_p^+ , and X . In particular,

$$X = \frac{\beta}{-i\Omega + \Gamma_{IT}} \frac{\bar{a}^* \sqrt{\eta}\Gamma}{i(\bar{\Delta} - \Omega) + \Gamma/2} s_p. \quad (10)$$

Here we defined an “induced transparency linewidth,” whose physical meaning will become clear in the next subsection, in particular, after Eq. (16),

$$\Gamma_{IT} = \gamma \left(1 + \frac{|\bar{a}|^2}{|\bar{a}_b|^2} \tilde{\chi}(\bar{\Delta}) \right), \quad (11)$$

where $|\bar{a}_b|^2$ represents the characteristic energy for optical bistability already introduced in Sec. II A, whereas the parameter,

$$\tilde{\chi}(\bar{\Delta}) \approx \frac{4\bar{\Delta}/\Gamma}{4\bar{\Delta}^2/\Gamma^2 + 1} \quad (12)$$

can be interpreted as an effective susceptibility for this nonlinear phenomenology [23] as it clearly appears from its plot in Fig. 3(a).

The physical meaning of Eq. (10) can be summarized as follows. The term on the right-hand side of the product represents the optical response of the cavity under external excitation in the absence of the induced transparency effect. This is described by a Lorentzian lineshape, centered at $\Omega = \bar{\Delta}$ and with full width at half maximum Γ . Conversely, the term on the left-hand side of the product is associated with the first-order response of the physical system. It also consists of a Lorentzian function, centered in $\Omega = 0$ and with halfwidth at half maximum Γ_{IT} .

Thus, the oscillation amplitude X [Fig. 3(b)] can be appreciably different from zero only if the control field is tuned in frequency within the optical resonator response ($\bar{\Delta} \sim \Gamma$), and the probe field is at the same time sufficiently close to the control frequency ($\Omega \sim \Gamma_{IT}$). In the case that the first-order system response is much slower than the optical one ($\gamma \ll \Gamma$) as we will assume from now on, the overall spectral response of X is dominated by the linewidth Γ_{IT} and can be itself approximated by a Lorentzian curve. Note that the width of the oscillation curve Γ_{IT} (i.e., the effective dissipation rate) depends on the control energy $|\bar{a}|^2$. In particular, it increases ($\Gamma_{IT} > \gamma$) in the blue-detuning regime ($\bar{\Delta} > 0$), and it decreases ($0 < \Gamma_{IT} < \gamma$) in the red-detuning regime ($\bar{\Delta} < 0$). In both cases, for a given control energy $|\bar{a}|^2$, Γ_{IT} is

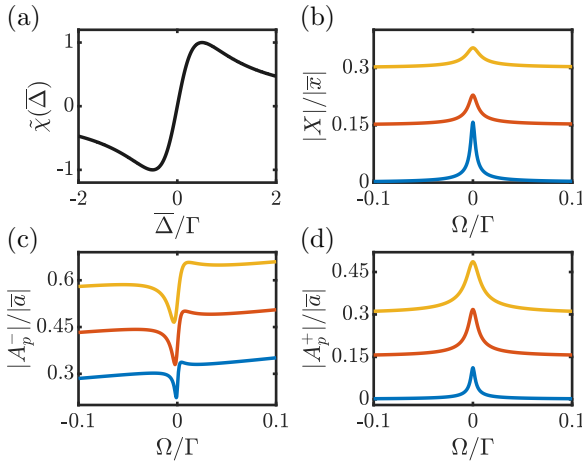


FIG. 3. (a) Susceptibility of the induced transparency as a function of the detuning between the control field and the shifted resonator mode frequencies. (b)–(d) Oscillation amplitude/Stokes and anti-Stokes sidebands amplitude as a function of the probe-control detuning frequency, Ω . The calculations were performed with system parameters $\gamma = 10^{-3}\Gamma$, $G = -10^{-1}\Gamma$, $\beta = 10^{-2}\Gamma$, and driving parameters $|s_p|^2 = 0.1|\bar{s}_a|^2$, $\bar{\Delta} = +\Gamma/2$, and $|\bar{a}|^2 = (|\bar{a}_b|^2, 3|\bar{a}_b|^2, 5|\bar{a}_b|^2)$ from the blue to the yellow curve, respectively. All curves are spaced by a vertical offset of 0.15 for clarity.

either maximized or minimized when $\bar{\Delta} = \pm\Gamma/2$. Thus, the effective dissipation rate of the first-order system is controlled by the action of the strong control field. This behavior is typical of EIT phenomenology, and it was also reported in connection with several EIT analogs in the literature, such as Refs. [11,12].

Given the expressions (10) and (11), the anti-Stokes A_p^+ field can be analytically derived from Eq. (9b),

$$A_p^+ \approx \frac{1}{i\Omega + \Gamma_{IT}} \frac{iG\beta\bar{a}^2\sqrt{\eta\Gamma}}{\bar{\Delta}^2 - \Omega^2 + \Gamma^2/4} s_p^*. \quad (13)$$

The overall spectral lineshape of A_p^+ is also a Lorentzian curve [see Fig. 3(d)], with half-width at half maximum Γ_{IT} . Briefly, the field amplitude A_p^+ can be interpreted as a sideband generated by the modulation of the control field inside the cavity by the oscillation X , and similar considerations as for the X solution lineshape apply.

A similar expression for the Stokes field amplitude A_p^- can be analytically derived from Eq. (9a),

$$A_p^- = \left(1 + \frac{1}{-i\Omega + \Gamma_{IT}} \frac{iG\beta|\bar{a}|^2}{i(\bar{\Delta} - \Omega) + \Gamma/2}\right) \times \frac{\sqrt{\eta\Gamma}}{i(\bar{\Delta} - \Omega) + \Gamma/2} s_p. \quad (14)$$

In this case, the coherent mixing between the input probe field and the sideband generated by the modulation of the control field produces an asymmetric Fano-type lineshape [see Fig. 3(c)].

3. Output signal

We will now employ the analytic expressions derived above to construct the output signal. In particular, within

an input-output formalism the output field can be expressed as [24]

$$s_{\text{out}}(t) = -\sqrt{\eta\Gamma}a(t), \quad (15)$$

in which one assumes that the outcoupling rate $\Gamma_{\text{out}} = \Gamma_{\text{in}} = \eta\Gamma$ is essentially the same as the input for the sake of simplicity and as it is common in many experimental situations. Being directly proportional to the intracavity field amplitude, the output field contains three frequency components, oscillating at the carrier (ω_c), Stokes ($\omega_c - \Omega$), and anti-Stokes ($\omega_c + \Omega$) frequencies, respectively. Note that all the components' amplitude and phase depend both on the control and on the probe fields.

Focusing our attention to potential technological applications (e.g., optical pulse delay), we will define an output signal based on the optical beating occurring on the output field intensity, i.e., $I(t) = |s_{\text{out}}(t)|^2$ where the output field amplitude is given by Eq. (15). This depends on all the frequency components involved, and it is explicitly given as

$$\begin{aligned} I(t) &= \eta\Gamma|\bar{a} + A_p^-e^{-i\Omega t} + A_p^+e^{+i\Omega t}|^2 \\ &= 2\eta\Gamma \text{Re}\{\bar{a}^*A_p^- + \bar{a}A_p^{+*}\} \cos \Omega t \\ &\quad + 2\eta\Gamma \text{Im}\{\bar{a}^*A_p^- + \bar{a}A_p^{+*}\} \sin \Omega t + \dots, \end{aligned}$$

where in the last two lines we considered only the components oscillating at frequency Ω . As aforementioned, the latter can be seen as the beating frequency between control and probe fields. Although an optical beating is observable also on the input field intensity $|s_{\text{in}}(t)|^2$, the amplitude and phase of this oscillation on $|s_{\text{out}}(t)|^2$ depend exclusively on the underlying induced transparency phenomenology.

In the frequency domain, the oscillation on the output intensity can be expressed in the complex form $\tilde{I}(\Omega) = 2\eta\Gamma(\bar{a}^*A_p^- + \bar{a}A_p^{+*})$. From comparison with Eqs. (9c) and (10), this is finally calculated as

$$\tilde{I}(\Omega) = \left(1 - \frac{\Gamma_{IT} - \gamma}{-i\Omega + \Gamma_{IT}}\right) \frac{2\bar{a}^*(\eta\Gamma)^{3/2}}{i(\bar{\Delta} - \Omega) + \Gamma/2} s_p. \quad (16)$$

In the blue- (red-) detuning regime, the multiplying term within brackets represents a Lorentzian dip (peak) of width Γ_{IT} and visibility $|\mathcal{V}|$, respectively, such that

$$\mathcal{V} = 1 - \frac{\gamma}{\Gamma_{IT}}, \quad (17)$$

where we have defined the visibility as the height of the dip (peak) spectral feature divided by the value of the unperturbed cavity response.

The amplitude of the output signal Eq. (16) is explicitly shown in Fig. 4 for different driving and detuning conditions. As is evidenced, the typical system response displays very narrow absorption or gain features within the broader Lorentzian response of the shifted resonator mode, similar to the phenomenology already observed for optomechanically coupled oscillators [12].

4. Phase response and group delay

The visibility of the induced absorption or gain phenomenon is directly related to the already defined linewidth Γ_{IT} . As we will see, this has a crucial role in the determination

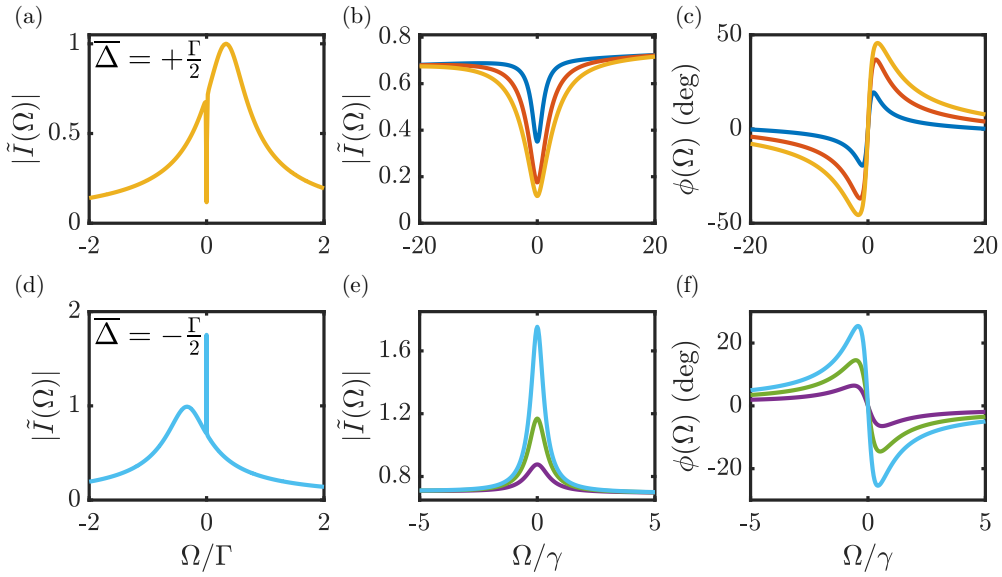


FIG. 4. Output signal amplitude (normalized by the peak cavity response at $\Omega = \bar{\Delta}$) and phase in blue- (a)–(c) and red- (d)–(f) detuning regimes, respectively. The calculations assume the following physical parameters: $\gamma = 10^{-3}\Gamma$, $G = -10^{-1}\Gamma$, $\beta = 10^{-2}\Gamma$, and driving parameters $\bar{\Delta} = +\Gamma/2$, $|\bar{a}|^2 = (|\bar{a}_b|^2, 3|\bar{a}_b|^2, 5|\bar{a}_b|^2)$ (a)–(c); $\bar{\Delta} = -\Gamma/2$, $|\bar{a}|^2 = (0.2|\bar{a}_b|^2, 0.4|\bar{a}_b|^2, 0.6|\bar{a}_b|^2)$ (d)–(f).

of the phase response, and, hence, the associated group delay or advance.

First, the phase associated with Eq. (16) can be expressed as

$$\phi(\Omega) = -\arg\{\tilde{I}(\Omega)\} \approx \arctan\left\{\frac{\Omega(\Gamma_{IT} - \gamma)}{\Omega^2 + \gamma\Gamma_{IT}}\right\}, \quad (18)$$

where we neglected the bare resonator phase response. Note that the above definition assumes an optical beating in the form $I(t) = |\tilde{I}| \cos(\Omega t + \phi)$. The above function has absolute maximum and minimum in $\Omega = \pm\sqrt{\gamma\Gamma_{IT}}$, which corresponds to a phase shift,

$$\phi^{\text{peak}} = \pm \arctan\left\{\frac{1}{2} \frac{\gamma}{\sqrt{1-\gamma}}\right\}. \quad (19)$$

The effect of this dispersive system response on an optical pulse can be qualitatively understood as a phase shift, i.e., given by Eq. (18), acting on all its frequency components. In the region where $|\Omega| < \sqrt{\gamma\Gamma_{IT}}$, the phase response is approximately linear, and the overall effect on the optical pulse is a time delay or advance. This group delay is hereby defined as

$$\tau_g(\Omega) = -\frac{d\phi}{d\Omega} \xrightarrow{\Omega \rightarrow 0} -\frac{\gamma}{\gamma}, \quad (20)$$

which absolute value is clearly maximized for $\Omega \sim 0$. Note that in the blue-detuning regime the delay is negative (group advance), and it asymptotically reaches the value of $\tau_g^{\text{min}} = -1/\gamma$ for unit visibility. Conversely, in the red-detuning regime the delay is positive, and it diverges for $\Gamma_{IT} \rightarrow 0$. The calculated phase response for different driving and detuning conditions is shown in Figs. 4(c) and 4(f), and its phenomenology is consistent with the one commonly observed in bulk fast- and slow-light media [3].

The visibility \mathcal{V} and the associated peak phase shift ϕ^{peak} as defined by Eqs. (17) and (19), respectively, are plotted in Fig. 5 as a function of the cavity energy $|\bar{a}|^2$ and detuning

parameter $\tilde{\chi}$. The red- and blue-detuning regimes are explicitly indicated in the panels, respectively.

III. APPLICATION TO SEMICONDUCTOR MICROCAVITIES

The model and the solutions discussed so far are general, the only requirement being the coupling of a single-mode Kerr-type nonlinear oscillator to a dissipative first-order

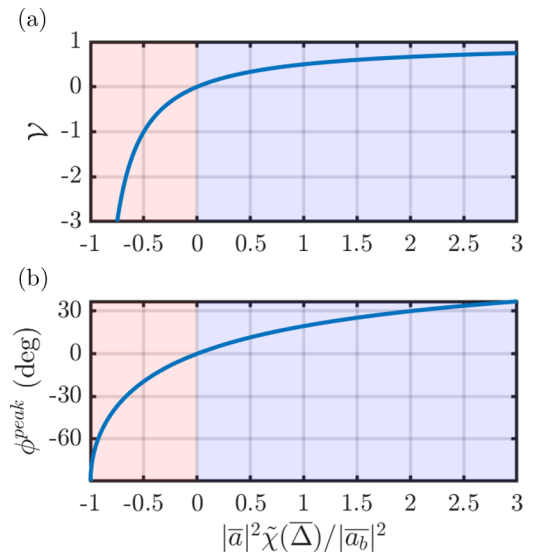


FIG. 5. (a) Calculated trend for dip visibility as a function of the $|\bar{a}|^2\tilde{\chi}$ product, which value is determined by the control field intensity and detuning conditions. Negative values indicate a peak spectral feature. (b) Calculated trend for peak phase shift Eq. (19). The + sign, associated with the local maximum/minimum at $\Omega = +\sqrt{\gamma\Gamma_{IT}}$, was chosen. Red (blue) shaded regions are associated with the respective detuning regimes.

system. We have shown that induced absorption and gain phenomena can easily be evidenced in such systems as well as the associated group advance or delay.

We will now discuss the actual relevance of these results in practical realizations of this model. In particular, we consider conventional semiconductor microcavities in standard material platforms, such as silicon or III–V alloys, which are typically characterized by intensity-dependent effective nonlinearities, such as thermo-optic or free-carrier dispersion effects [25].

A. Thermo-optically induced transparency

1. Induced absorption and gain from thermo-optic nonlinearity

The TO nonlinear effect consists of a local variation of the refractive index due to the heating of an optical medium. In a semiconductor microcavity, a variation of the refractive index in the region where the field is localized translates into a variation of the resonance frequency. According to first-order perturbation theory, the resonance shift is given by [21]

$$\frac{\Delta\omega_0}{\omega_0} = -\frac{\Delta n}{n} = -\frac{1}{n} \frac{dn}{dT} \Delta T = \alpha \Delta T, \quad (21)$$

where for simplicity we assumed the temperature variation ΔT (with respect to room temperature) to be uniform over the whole cavity region and the field to be completely confined within the optical medium subject to the TO effect. Moreover, we are neglecting any other temperature-related effect (e.g., thermal expansion) which may induce, by any extrinsic mechanisms, a further shift of the resonance wavelength. Although these mechanisms are usually present in real-world microresonators, their impact can be quantified either from first principles [26] or by experimental measurement [27] of the resonance shift. The overall effect can be modeled in the limit of a small temperature variation by a correction to the TO coefficient α .

In the case in which linear absorption is the origin of the heating, and the optical intensity is time varying, the temperature variation is also time dependent. Its dynamics is then governed by the following rate equation [21]:

$$C_p \frac{d}{dt} \Delta T(t) = \Gamma_{\text{abs}} |a(t)|^2 - K \Delta T(t), \quad (22)$$

where C_p is an effective heat capacity, $\Gamma_{\text{abs}} = \eta_{\text{abs}} \Gamma$ is the optical absorption rate, and K is an effective heat conductance.

With these definitions, it is straightforward to recast Eqs. (1) and (2) to appropriately describe the thermo-optic dynamics. This can be accomplished by formally identifying $x(t) = \Delta T(t)$, $\beta = \Gamma_{\text{abs}}/C_p$, $\gamma = K/C_p$, and $G = \omega_0 \alpha$. As a consequence, all of the results discussed in Sec. II can be applied to single-mode optical resonators subject to linear absorption and the TO nonlinear shift of its resonance frequency.

Although thermal bistability is a well-known phenomenon in the domain of optical microcavities [21,28], thermo-optically induced transparency (TOIT) has been demonstrated only very recently [18,19], and it can be regarded as a peculiar example of induced transparency from a first-order dynamical system obtained through mechanisms discussed in the previous section. Within this context, the previously introduced

characteristic bistability energy is given by

$$|\bar{a}_b|^2 = -\frac{\gamma \Gamma}{2G\beta} = -\frac{K}{2Q\alpha\eta_{\text{abs}}}, \quad (23)$$

where $Q = \omega_0/\Gamma$ is the quality factor of the bare cavity resonance and $\eta_{\text{abs}} = \Gamma_{\text{abs}}/\Gamma$ is the absorption efficiency, i.e., the fraction of optical loss associated to light absorption. Note that the formal expression of the bistability energy above does not depend on any dynamical parameter (such as γ) as it describes the static behavior of the resonator in the presence of a control field with constant amplitude.

The value of $|\bar{a}_b|^2$ can be very small for integrated resonators with values of less than 1 fJ for silicon photonic crystal (PhC) cavities [28] and few femtojoules in microring resonators [29] to name some of the most widespread microcavity designs. Nevertheless, this nonlinearity has already been explored in the past for applications, such as low-power all-optical switching [30]. In the framework of TOIT, this translates in a very low threshold for the activation of the observed phenomenology [18].

The dynamical properties of the induced absorption or gain are governed by the thermal decay rate γ . As Eq. (11) suggests, the already defined induced transparency linewidth Γ_{IT} will be (in most practical cases) quite close to γ as an order of magnitude. This value is, in general, larger for smaller sized microcavities as highlighted by recent experiments. In particular, a linewidth in the submegahertz range has been reported in the case of TOIT measured in an integrated silicon PhC cavity [18] and a sensibly slower dynamics in the case of a bulk Fabry-Pérot system with a linewidth of the order of 100 Hz [19]. Indeed, typical orders of magnitude for integrated resonators are in the range of $\gamma/2\pi \sim 1$ MHz for both silicon PhC cavities [28,31] and microring resonators [32,33], respectively.

2. Modeling thermal diffusion

The model for the TOIT effect detailed in the previous paragraph describes the thermal dynamics by means of a single temperature offset $\Delta T(t)$ associated with a discrete thermal decay rate $\gamma = K/C_p$ by means of the first-order differential equation (22). Although this discretization allows to find a direct correspondence with the general case, i.e., Eqs. (1) and (2), it is usually quite a rough approximation for the modeling of actual system dynamics. Here, to complete this section, we provide a generalization of TOIT based on a more accurate model of heat diffusion within a microstructure.

In the most general description, temperature is an intensive time-dependent quantity governed by the heat diffusion equation,

$$\rho c_p \frac{\partial}{\partial t} T(\mathbf{r}, t) + \nabla[-\kappa \nabla T(\mathbf{r}, t)] = \frac{\partial}{\partial t} u(\mathbf{r}, t), \quad (24)$$

where ρ is the medium density, c_p is the mass specific heat, κ is the thermal conductivity, and $\frac{\partial u}{\partial t}$ is a source term describing the heat flux density towards the system, in this case associated with the absorbed optical power. In this context, Eq. (22) represents a discretized version of the heat diffusion equation where the temperature offset with respect to room temperature is considered uniform over a finite volume region, i.e., $\Delta T(\mathbf{r}, t) \rightarrow \Delta T(t)$. In this “lumped elements” model, the

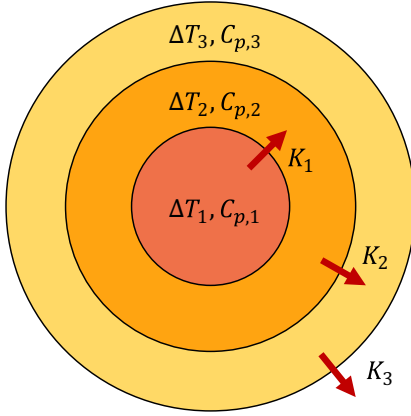


FIG. 6. Discretized heat diffusion model. Each shell is characterized by a heat-capacity $C_{p,i}$, and it exhibits a heat diffusion constant K_i and a temperature offset ΔT_i with respect to the next outer shell.

intensive physical quantities, c_p and κ , appearing in Eq. (24), are replaced by extensive ones, respectively C_p and K .

Following an approach already suggested in previous works [21,34,35], a more accurate description of the problem can be formulated by slicing the thermal distribution into n concentric regions, whose definition depends on the detailed geometrical aspects of the system. A schematic is reported in Fig. 6 for completeness. Each region is labeled from 1 to n such that $i = 1$ is the innermost thermal shell where the field is mainly confined, and $i = n$ is the outermost one. The i th region is characterized by a heat-capacity $C_{p,i}$, an effective temperature offset ΔT_i with respect to the $(i + 1)$ -th one, and a heat diffusion constant K_i towards it. Given these definitions, Eqs. (1) and (2) are straightforwardly generalized as follows:

$$\frac{d}{dt}a(t) = \left(i\omega_0 - \frac{\Gamma}{2}\right)a(t) + iG \Delta T(t)a(t) + \sqrt{\eta\Gamma}s_{\text{in}}(t), \quad (25a)$$

$$\frac{d}{dt}\Delta T_1(t) = \beta|a(t)|^2 - \gamma_{1,1}\Delta T_1(t), \quad (25b)$$

$$\frac{d}{dt}\Delta T_2(t) = \gamma_{1,2}\Delta T_1(t) - \gamma_{2,2}\Delta T_2(t), \quad (25c)$$

...

$$\frac{d}{dt}\Delta T_n(t) = \gamma_{n-1,n}\Delta T_{n-1}(t) - \gamma_{n,n}\Delta T_n(t), \quad (25d)$$

where the overall temperature offset experienced by the field is $\Delta T(t) = \sum_{i=1}^n \Delta T_i(t)$, whereas the rates connecting different regions are defined $\gamma_{i,j} = K_i/C_{p,j}$ and $\beta = \Gamma_{\text{abs}}/C_{p,1}$. With these definitions and the assumptions made in the previous paragraph, Eqs. (25) describe with arbitrarily high accuracy any thermal diffusion process that is consistent with the symmetry and geometrical details of the problem.

In the presence of a monochromatic control field, a solution formally similar to Eq. (4) can be derived

$$\bar{a} = \frac{\sqrt{\eta\Gamma}}{i(\omega - \omega_0 - G\bar{\Delta T}) + \Gamma/2} \bar{s}_{\text{in}}, \quad (26a)$$

$$\bar{\Delta T} = \frac{\Gamma_{\text{abs}}}{K} |\bar{a}|^2, \quad (26b)$$

where $\bar{\Delta T} = \sum_{i=1}^n \bar{\Delta T}_i$ is the overall temperature offset and $K = (\sum_{i=1}^n K_i^{-1})^{-1}$ is the total series conductance. With these definitions, the steady-state result obtained from the generalized model is formally identical to the one obtained in the simplified one nicely. This result justifies *a posteriori* the simplified description in the steady-state condition, which can be effectively described by a single temperature offset ΔT and a single heat conductance K .

Following the steps discussed in Appendix A, it is possible to derive an analytic expression for the temperature oscillation amplitude $T(\Omega)$ and the output signal $\tilde{I}(\Omega)$ in the framework of this generalized model,

$$T(\Omega) = \xi(\Omega) \frac{\beta}{-i\Omega + \Gamma_{IT}(\Omega)} \frac{\bar{a}^* \sqrt{\eta\Gamma}}{i(\bar{\Delta} - \Omega) + \Gamma/2} s_p, \quad (27)$$

$$\tilde{I}(\Omega) = \left(1 - \frac{\Gamma_{IT}(\Omega) - \gamma_{1,1}}{-i\Omega + \Gamma_{IT}(\Omega)}\right) \frac{2\bar{a}^* (\eta\Gamma)^{3/2}}{i(\bar{\Delta} - \Omega) + \Gamma/2} s_p, \quad (28)$$

in which

$$\Gamma_{IT}(\Omega) = \gamma_{1,1} \left(1 + \frac{|\bar{a}|^2}{|\bar{a}_b|^2} \xi'(\Omega) \tilde{\chi}(\bar{\Delta})\right), \quad (29)$$

where $\xi'(\Omega) = K\xi(\Omega)/K_1$ and

$$\xi(\Omega) = 1 + \sum_{j=2}^n \left(\prod_{i=2}^j \frac{\gamma_{i-1,i}}{-i\Omega + \gamma_{i,i}} \right). \quad (30)$$

The latter expression clearly displays a recursive hierarchical structure. Note that $\Gamma_{IT}(\Omega)$ is now a frequency-dependent quantity, and it cannot be simply interpreted as a linewidth as done before in connection with Eq. (11). However, this quantity still provides relevant information for the description of the induced transparency visibility. In fact, the thermal response function $\xi(\Omega)$ (plotted in Fig. 7) and its normalized form $\xi'(\Omega)$ contain all the information about the thermal process dynamics, quantified by the decay rates $\gamma_{i,j}$. A comparison between this result (by assuming $n = 3$) and the simplified model with a single thermal decay time is explicitly shown in Fig. 7. As it can be noted, the simplified model is a reasonably good approximation for the quantitative estimation of the zero-detuning response, but it fails to correctly capture the detailed lineshapes, which may significantly deviate from a single Lorentzian.

Similar figures of merit as for the general model can be derived. In particular, the expression for the visibility is basically the same as the one previously introduced in Eq. (17), and it reads

$$\mathcal{V} = 1 - \frac{\gamma_{1,1}}{\Gamma_{IT}(0)}. \quad (31)$$

In contrast, the expressions for the phase and the group delay become more complicated in this case than the ones introduced in Eqs. (18) and (20), respectively. A full derivation is detailed in Appendix A for completeness. In particular, for small values of Ω it is found that the group delay as a function of \mathcal{V} shows a trend similar to the one given by Eq. (20),

$$\tau_g(\Omega \rightarrow 0) \approx -\frac{\mathcal{V}}{\gamma_{\text{eff}}} \quad (32)$$

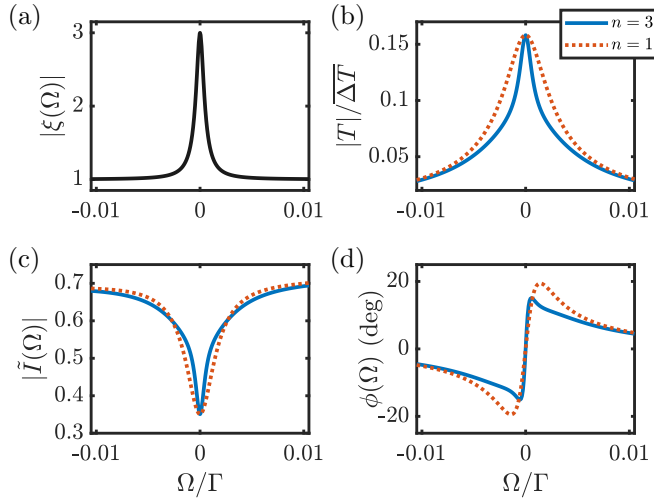


FIG. 7. Comparison between the TOIT response for the generalized (blue solid line) and the simplified (red dashed line) models, respectively. (a) Thermal response function $\xi(\Omega)$ as a function of the probe-control detuning. (b) Temperature oscillation amplitude. (c) Amplitude and (d) phase response for the output signal. The calculation assumes the following parameters: $G = -10^{-1}\Gamma$, $\beta = 10^{-2}\Gamma$, $\bar{\Delta} = +\Gamma/2$, and $|\bar{a}|^2 = |\bar{a}_b|^2$. For the nonrefined model ($n = 1$) we chose $\gamma = 10^{-3}\Gamma$, whereas for the refined model ($n = 3$) we chose $\gamma_{1,1} = 3 \times 10^{-3}\Gamma$, $\gamma_{1,2} = \gamma_{2,2} = \gamma_{1,1}/4$, $\gamma_{2,3} = \gamma_{3,3} = \gamma_{1,1}/8$. Note that by this choice of parameters, the static temperature offset $\bar{\Delta T}$ is the same in both scenarios.

where γ_{eff} is an effective thermal decay rate, which is a function of the $\gamma_{i,j}$ parameters. The minimum (negative) group delay achieved asymptotically in the blue-detuning regime is then given by $\tau_g^{\min} = -1/\gamma_{\text{eff}}$. As an example, for the case of $n = 3$, this is given by

$$\tau_g^{\min} = -\frac{\gamma_{1,2}/\gamma_{2,2}^2 + (\gamma_{2,2} + \gamma_{3,3})\gamma_{1,2}\gamma_{2,3}/\gamma_{2,2}^2\gamma_{3,3}^2}{1 + \gamma_{1,2}/\gamma_{2,2} + \gamma_{1,2}\gamma_{2,3}/\gamma_{2,2}\gamma_{3,3}}.$$

B. Free-carrier induced transparency

Free-carrier dispersion (FCD) is an ubiquitous phenomenon in semiconductor microcavities, and its behavior has been extensively studied in silicon devices [25,36]. It consists of a modification of the refractive index induced by the presence of hot carriers in the valence or conduction bands of a semiconductor material, which can be modeled by a simple Drude theory to a first approximation [37].

If a localized resonant mode is confined in a region affected by FCD, the associated resonance shift will be, to first-order [26],

$$\frac{\Delta\omega_0}{\omega_0} = -\frac{\Delta n}{n} = -\frac{1}{n} \frac{dn}{dN} N = \zeta N, \quad (33)$$

where N is the effective carrier density, which we assume to have a uniform distribution over the whole cavity region. We also assume the field to be completely confined within the optical medium subject to FCD. The FCD coefficient ζ is typically positive, i.e., the presence of a carrier density yields a blueshift of the cavity resonance.

If the population of free carriers is the result of an excitation by the electromagnetic field associated with the localized mode, FCD phenomenologically behaves as an effective nonlinearity, similar to the TO effect but with an opposite sign. Specifically, if the free-carrier population is generated by linear absorption (e.g., absorption from defect states), the free-carrier dynamics is described by the following rate equation [35]:

$$\frac{d}{dt}N(t) = \frac{\Gamma_{\text{abs}}}{V\hbar\omega}|a(t)|^2 - \frac{1}{\tau_c}N(t), \quad (34)$$

where ω is the electromagnetic-field frequency Γ_{abs} is the absorption rate, τ_c is the free-carrier recombination lifetime, and V is an effective volume occupied by the free carriers.

Again, it is immediate to recast Eqs. (1) and (2) to properly describe the FCD dynamics. Specifically, here we formally identify $x(t) = N(t)$, $\beta = \Gamma_{\text{abs}}/V\hbar\omega$, $\gamma = 1/\tau_c$, and $G = \omega_0\zeta$. As a consequence, the predicted phenomenology described in Sec. II is observable in semiconductor optical cavities affected by linear absorption and FCD. In contrast to TOIT, this phenomenon, which we will refer as free-carrier induced transparency (FCIT) has not been predicted, nor experimentally reported, to date. The resonance shift induced by FCD has been investigated in the past mainly in the framework of fast all-optical switching [38,39]. In this context, the FCD mechanism typically consists in a much faster response time and a comparable characteristic bistability energy as compared to the TO effect. Similar considerations then apply to FCIT as compared to TOIT.

In fact, the characteristic bistability energy is here given by

$$|\bar{a}_b|^2 = -\frac{\gamma\Gamma}{2G\beta} = -\frac{\hbar V}{2\tau_c\zeta\eta_{\text{abs}}}, \quad (35)$$

where we assumed $\omega \approx \omega_0$. Note that, since the sign of interaction is opposite to the case of the TO effect (here, $G > 0$), FCD gives rise to a reversed sawtooth-shaped response in the steady-state scenario as compared to the one already reported in Fig. 2. In practical cases, a combination of TO and FCD nonlinearities may occur, which may manifest into the dynamical cavity response. In some circumstances, this gives rise to an unstable behavior, such as self-pulsations as already reported [33].

In the case of FCIT, the most remarkable consequence of the reversed sign of the interaction is an opposite phenomenology when compared to the TOIT scenario: in the blue-detuning regime ($\bar{\Delta} > 0$), a FCIT peak is expected, associated with a narrowing of the induced transparency linewidth ($\Gamma_{IT} < \gamma$). Conversely, a FCIT dip with associated linewidth broadening ($\Gamma_{IT} > \gamma$) is expected in the red-detuning regime ($\bar{\Delta} < 0$). Apart from this difference, the phenomenology to be expected with these two nonlinear processes is essentially identical, and a generalized model accounting for the spatial carrier diffusion can be formulated with an approach similar to the one presented in the previous paragraph. The formulation of such a model, based on the carrier diffusion equation rather than the heat diffusion law, is straightforward but goes beyond the scope of the present paper.

In practical semiconductor devices, FCIT exhibits a higher characteristic bistability energy $|\bar{a}_b|^2$ as compared to TOIT. The existing literature reports all-optical switching energy values ranging from ~ 100 fJ to ~ 10 pJ in silicon PhC

cavities [39,40], and sub-femtojoules values reported for III–V devices exploiting the band-filling dispersion nonlinearity [38], an analogous but physically different dispersive mechanism to FCD. Switching energies on the order of 1 pJ have been reported for microring resonators [41].

C. Discussion and comparison

We have shown two different examples of effective nonlinearities that could be treated within the unified framework introduced in the previous section, yielding remarkably similar phenomenology associated with EIT physics. In particular, applications requiring slow and fast light may benefit from the engineering of such first-order dynamical systems.

In this respect, it is worth recalling that a fast response time is particularly beneficial for applications requiring a wide operational bandwidth, such as fast optical memories. However, the overall delay (or advance) achievable is limited, in general, by a key figure of merit, such as the delay-bandwidth product $\Delta t \Delta \omega \leq 2\pi$. Hence, the narrower the bandwidth, the larger the delay time that could be achieved. Within this context, it is worth stressing that TOIT allows great flexibility offered at a design level by the engineering of the resonator thermal properties [35]. Another key feature of TOIT is the possibility to overcome the delay-bandwidth limit by cascading multiple resonators [42]. This solution is practically hindered in many EIT analogs due to the tight requirements of matching an optical and an atomic, mechanical or acoustic resonance, whereas it would be relatively easy to implement in TOIT-based devices.

Despite the higher threshold energy as compared to TOIT, FCIT has significant advantages in terms of bandwidth, which is determined by the free-carrier lifetime τ_c rather than the thermal decay time. Typical values can be on the order of 100 ps for PhC cavities [25,43] and on the order of 1 ns for whispering gallery mode resonators [44]. In both cases, τ_c can be further reduced by ion implantation [31,41]. The resulting induced transparency linewidth and, hence, slow or fast light bandwidth, lies in the gigahertz range, opening a pathway to applications, such as broadband delay lines and optical memories, even at room temperature and in cost-effective material platforms. Finally, although it is worth noting that the maximum delay or advance theoretically achievable with FCIT would be much lower than the TOIT case, also FCIT can be easily cascaded along multiple resonators, thus, considerably extending the potential delay achievable above these limits.

IV. SUMMARY AND OUTLOOK

We have presented a general model describing a physical system governed by first-order dynamics and coupled to a single-mode optical resonator, showing how its solution can lead to the observation of analog EIT phenomenology in a driving configuration in which a weak probe beam is superimposed to a strong control field. From a set of two coupled equations of motion, we have derived analytic expressions for the key physical quantities involved both in the steady state and in a control and probe scenario. For the latter case, we showed that induced transparency emerges as an interference effect between the cavity control and probe fields, mediated by the effective interaction provided

by the first-order dynamical system. This results in induced absorption (spectral hole) in the control-cavity blue-detuning regime ($\bar{\Delta} > 0$) and induced gain or amplification (spectral antihole) in the red-detuning regime ($\bar{\Delta} < 0$) for a Kerr-type effective interaction ($G < 0$). The former case is associated with fast light and the broadening of the induced transparency linewidth, whereas the latter case is associated with slow light and the narrowing of the induced transparency feature. The relevant figures of merit, including the spectral linewidth Γ_{IT} , the visibility \mathcal{V} , and the group delay τ_g were explicitly derived, and linked to the properties of the physical system, such as the characteristic optical bistability energy $|\bar{a}_b|^2$ and the first-order system damping rate γ .

In Sec. III, we discussed the specific correspondence of this general model to the physics of semiconductor microcavities subject to effective Kerr-type nonlinearities. In particular, our focus was on two different dispersive mechanisms, namely, the thermo-optic effect and the free-carrier dispersion, which are typical of several semiconductor photonic devices. We evidenced how both effects can be driven by the absorption of the cavity field, and they can, thus, be regarded as effective Kerr-type nonlinearities, each described by a characteristic first-order differential equation. The resulting induced transparency effects are theoretically predicted to yield a group advance or delay in the microsecond range for TOIT and in the nanosecond range for FCIT both hardly achieved on chip by current photonic technology [15]. As a comparison, a microsecond-scale delay achieved in an on-chip delay line would require an ~ 100 -m-long integrated waveguide with the current silicon photonics technology. Moreover, the two effects are associated with operational bandwidths in the megahertz and gigahertz ranges, respectively, which could be further increased by cascading multiple resonators without the need to match any mechanical or acoustic resonance. Furthermore, the transparency bandwidth could be controlled, in principle, by engineering the thermal or free-carrier properties of the microstructured resonators, for instance, by heat diffusion design [35] or ion bombardment [40]. It is also worth stressing that TOIT has recently been observed in two different experimental scenarios [18,19], whereas FCIT has not been reported at time of writing, which we believe will stimulate new experimental research in this direction.

Finally, the general and unified framework presented in this paper can be extended to other physical systems displaying a first-order response and coupled to a single-mode oscillator, opening a pathway towards the demonstration of generalized induced transparency analogs and the achievement of slow light in yet unforeseen platforms, thus, revealing novel viable approaches towards the realization of optical and quantum memories.

ACKNOWLEDGMENTS

This work was partly supported by the EU H2020 QuantERA ERA-NET Cofund in Quantum Technologies Project CUSPIDOR, cofunded by the Italian Ministry of Education, University and Research (MIUR), and by MIUR through the “Dipartimenti di Eccellenza Program”, Grant 2018-2022. Several useful discussions on transparency phenomena and thermo-optically induced transparency are acknowledged over the years with S. Iadanza, A. Imamoğlu, D. Nigro, M. F. Santos, S. Schulz, and G. Urbinati.

APPENDIX: DERIVATION FOR THE REFINED TOIT MODEL

Following the steps already discussed in Sec. II B, we will now derive the linearized equations of motion in the hypothesis of a weak probe field. The procedure is formally identical to the previous one for what concerns the field amplitude, whereas for the effective temperature the following additional assumptions are made:

$$\Delta T_i(t) = \overline{\Delta T}_i + \delta T_i(t), \quad (\text{A1a})$$

$$\delta T_i(t) = T_i e^{-i\Omega t} + T_i^* e^{+i\Omega t}, \quad (\text{A1b})$$

where

$$\overline{\Delta T} = \sum_{i=1}^n \overline{\Delta T}_i, \quad \delta T = \sum_{i=1}^n \delta T_i, \quad T = \sum_{i=1}^n T_i.$$

The linearized equations of motion, thus, read

$$\frac{d}{dt} \delta a(t) = \left(i\bar{\omega}_0 - \frac{\Gamma}{2} \right) \delta a(t) + iG, \bar{a} \delta T(t) + \sqrt{\eta\Gamma} \delta s_{\text{in}}(t), \quad (\text{A2a})$$

$$\frac{d}{dt} \delta T_1(t) = \beta [\bar{a}^* \delta a(t) + \bar{a} \delta a^*(t)] - \gamma_{1,1} \delta T_1(t), \quad (\text{A2b})$$

$$\frac{d}{dt} \delta T_i(t) = \gamma_{i-1,i} \delta T_{i-1}(t) - \gamma_{i,i} \delta T_i(t) \quad (i > 1). \quad (\text{A2c})$$

We note that the solution is formally similar to the one already found for a single thermal rate, Eqs. (9), although the temperature oscillation T now derives from all the temperature offsets T_i ,

$$A_p^- = \frac{iG\bar{a}T + \sqrt{\eta\Gamma} s_p}{i(\bar{\Delta} - \Omega) + \Gamma/2}, \quad (\text{A3a})$$

$$A_p^+ = \frac{iG\bar{a}}{i(\bar{\Delta} + \Omega) + \Gamma/2} T^*, \quad (\text{A3b})$$

$$T_1 = \frac{\beta}{-i\Omega + \gamma_{1,1}} [\bar{a}^* A_p^- + \bar{a} (A_p^+)^*], \quad (\text{A3c})$$

$$T_i = \frac{\gamma_{i-1,i}}{-i\Omega + \gamma_{i,i}} T_{i-1} \quad (i > 1). \quad (\text{A3d})$$

From the last equation,

$$T_i = \frac{\gamma_{i-1,i}}{-i\Omega + \gamma_{i,i}} \frac{\gamma_{i-2,i-1}}{-i\Omega + \gamma_{i-1,i-1}} \dots \frac{\gamma_{1,2}}{-i\Omega + \gamma_{2,2}} T_1 \quad (\text{A4})$$

which is valid for any $i > 1$. We can find a general relation between T and T_1 ,

$$T = \sum_{i=1}^n T_i = \xi(\Omega) T_1. \quad (\text{A5})$$

In the last step we defined the thermal response function $\xi(\Omega)$ such that

$$\begin{aligned} \xi(\Omega) = & 1 + \frac{\gamma_{1,2}}{-i\Omega + \gamma_{2,2}} \\ & + \frac{\gamma_{1,2}\gamma_{2,3}}{(-i\Omega + \gamma_{2,2})(-i\Omega + \gamma_{3,3})} \\ & + \dots + \prod_{i=2}^n \frac{\gamma_{i-1,i}}{-i\Omega + \gamma_{i,i}}. \end{aligned} \quad (\text{A6})$$

Note that $\xi(\Omega)$ has an absolute maximum in $\Omega = 0$ for which $\xi(0) = K_1/K$.

Applying this relation to the field components (A3), it is immediately possible to recover the formal expressions for the fields derived in the general model. In particular, by directly comparing with Eq. (A3c), we note that all the expressions previously obtained, including β and Γ_{IT} , can be generalized by substituting $\beta \rightarrow \xi(\Omega)\beta$ and $\gamma \rightarrow \gamma_{1,1}$. The resulting expressions for $T(\Omega)$, $\tilde{I}(\Omega)$, and $\Gamma_{IT}(\Omega)$ are reported in the main text.

In calculating the phase response associated to the output signal, we first subdivide $\xi(\Omega)$ in a real and an imaginary part,

$$\xi(\Omega) = \xi^r + i\xi^i,$$

$$\Gamma_{IT}(\Omega) = \gamma_{1,1} - \xi(\Omega)\zeta.$$

We then express

$$\tilde{I}(\Omega) = \frac{-i\Omega + \gamma_{1,1}}{-i\Omega(\Omega + \xi^i\sigma) + (\gamma_{1,1} - \xi^r\sigma)} \frac{2\bar{a}^*(\eta\Gamma)^{3/2}}{i(\bar{\Delta} - \Omega) + \Gamma/2} s_p,$$

where $\sigma = 2G\beta|\bar{a}|^2\bar{\Delta}/(\bar{\Delta}^2 + \Gamma^2/4)$. From the above expression, the phase can be approximated as

$$\phi(\Omega) \approx \arctan \frac{\Omega(\gamma_{1,1} - \xi^r\sigma) - \gamma_{1,1}(\Omega + \xi^i\sigma)}{\Omega(\Omega + \xi^i\sigma) + \gamma_{1,1}(\gamma_{1,1} - \xi^r\sigma)},$$

where we neglected the bare resonator phase response. We will now assume the peak group delay to have a functional form analogous to Eq. (20),

$$\tau_g(\Omega \rightarrow 0) \approx -\frac{\mathcal{V}}{\gamma_{\text{eff}}}, \quad (\text{A7})$$

where γ_{eff} is an effective decay rate that depends on the parameters $\gamma_{i,j}$. With this hypothesis and in the presence of linear dispersion at $\Omega \rightarrow 0$, the asymptotic group delay can then be expressed as

$$\begin{aligned} \tau_g &= \lim_{\Omega \rightarrow 0} -\frac{\phi}{\Omega} = -\frac{1}{\gamma_{1,1}} \left[1 - \frac{\gamma_{1,1}}{\Gamma_{IT}} (1 + \xi^i/\Omega\sigma) \right] \\ &\stackrel{\sigma \rightarrow \infty}{\approx} -\frac{1}{\xi^r} \frac{d\xi^i}{d\Omega} = \tau_g^{\text{min}}, \end{aligned}$$

where in the last step we assumed $\Gamma_{IT}(0) \gg \gamma_{1,1}$ and, thus, $\mathcal{V} \rightarrow 1$ in the blue-detuning regime. The final analytic result for the case $n = 3$ is reported in the main text.

- [1] M. Fleischhauer, A. Imamoglu, and J. P. Marangos, Electromagnetically induced transparency: Optics in coherent media, *Rev. Mod. Phys.* **77**, 633 (2005).
- [2] J. A. Souza, L. Cabral, R. R. Oliveira, and C. J. Villas-Boas, Electromagnetically-induced-transparency-related phenomena and their mechanical analogs, *Phys. Rev. A* **92**, 023818 (2015).
- [3] R. W. Boyd, Slow and fast light: Fundamentals and applications, *J. Mod. Opt.* **56**, 1908 (2009).
- [4] M. D. Lukin and A. Imamoglu, Controlling photons using electromagnetically induced transparency, *Nature (London)* **413**, 273 (2001).
- [5] K.-J. Boller, A. Imamoglu, and S. E. Harris, Observation of Electromagnetically Induced Transparency, *Phys. Rev. Lett.* **66**, 2593 (1991).
- [6] L. V. Hau, S. E. Harris, Z. Dutton, and C. H. Behroozi, Light speed reduction to 17 metres per second in an ultracold atomic gas, *Nature (London)* **397**, 594 (1999).
- [7] A. Faraon, I. Fushman, D. Englund, N. Stoltz, P. Petroff, and J. Vuckovic, Dipole induced transparency in waveguide coupled photonic crystal cavities, *Opt. Express* **16**, 12154 (2008).
- [8] D. Brunner, B. D. Gerardot, P. A. Dalgarno, G. Wüst, K. Karrai, N. G. Stoltz, P. M. Petroff, and R. J. Warburton, A coherent single-hole spin in a semiconductor, *Science* **325**, 70 (2009).
- [9] Q. Xu, S. Sandhu, M. L. Povinelli, J. Shakyia, S. Fan, and M. Lipson, Experimental Realization of an On-Chip All-Optical Analogue to Electromagnetically Induced Transparency, *Phys. Rev. Lett.* **96**, 123901 (2006).
- [10] N. Papasimakis, V. A. Fedotov, N. I. Zheludev, and S. L. Prosvirnin, Metamaterial Analog of Electromagnetically Induced Transparency, *Phys. Rev. Lett.* **101**, 253903 (2008).
- [11] S. Weis, R. Riviere, S. Deléglise, E. Gavartin, O. Arcizet, A. Schliesser, and T. J. Kippenberg, Optomechanically induced transparency, *Science* **330**, 1520 (2010).
- [12] A. H. Safavi-Naeini, T. P. M. Alegre, J. Chan, M. Eichenfield, M. Winger, Q. Lin, J. T. Hill, D. E. Chang, and O. Painter, Electromagnetically induced transparency and slow light with optomechanics, *Nature (London)* **472**, 69 (2011).
- [13] C. H. Dong, Z. Shen, C. L. Zou, Y. L. Zhang, W. Fu, and G. C. Guo, Brillouin-scattering-induced transparency and non-reciprocal light storage, *Nat. Commun.* **6**, 6193 (2015).
- [14] J. Kim, M. C. Kuzyk, K. Han, H. Wang, and G. Bahl, Non-reciprocal Brillouin scattering induced transparency, *Nat. Phys.* **11**, 275 (2015).
- [15] T. Alexoudi, G. T. Kanellos, and N. Pleros, Optical RAM and integrated optical memories: A survey, *Light Sci. Appl.* **9**, 91 (2020).
- [16] H. Pichler, S. Choi, P. Zoller, and M. D. Lukin, Universal photonic quantum computation via time-delayed feedback, *Proc. Natl. Acad. Sci. USA* **114**, 11362 (2017).
- [17] G. S. Agarwal and S. Huang, Electromagnetically induced transparency in mechanical effects of light, *Phys. Rev. A* **81**, 041803(R) (2010).
- [18] M. Clementi, S. Iadanza, S. Schulz, G. Urbinati, D. Gerace, L. O'Faolain, and M. Galli, Thermo-optically induced transparency in a photonic chip, *Light Sci. Appl.* **10** (2021).
- [19] J. Ma, J. Qin, G. T. Campbell, R. Lecamwasam, K. Sripathy, J. Hope, B. C. Buchler, and P. K. Lam, Photothermally induced transparency, *Sci. Adv.* **6**, eaax8256 (2020).
- [20] M. Soljačić, M. Ibanescu, S. G. Johnson, Y. Fink, and J. D. Joannopoulos, Optimal bistable switching in nonlinear photonic crystals, *Phys. Rev. E* **66**, 055601(R) (2002).
- [21] T. Carmon, L. Yang, and K. J. Vahala, Dynamical thermal behavior and thermal self-stability of microcavities, *Opt. Express* **12**, 4742 (2004).
- [22] L. A. Lugiato, Theory of Optical Bistability, *Progress in Optics* **21**, 69 (1984).
- [23] Note that the full expression for the susceptibility is, in general, complex valued: $\tilde{\chi}(\bar{\Delta}) = \frac{4\Delta/\Gamma}{4(\bar{\Delta}^2 - \Omega^2)/\Gamma^2 - i4\Omega/\Gamma + 1}$. The approximation assumes $|\Omega| \ll \Gamma/2$.
- [24] M. Aspelmeyer, T. J. Kippenberg, and F. Marquardt, Cavity optomechanics, *Rev. Mod. Phys.* **86**, 1391 (2014).
- [25] M. Borghi, C. Castellani, S. Signorini, A. Trenti, and L. Pavesi, Nonlinear silicon photonics, *J. Opt.* **19**, 093002 (2017).
- [26] P. E. Barclay, K. Srinivasan, and O. Painter, Nonlinear response of silicon photonic crystal micresonators excited via an integrated waveguide and fiber taper, *Opt. Express* **13**, 801 (2005).
- [27] K. Debnath, M. Clementi, T. T. D. Bucio, A. A. Z. Khokhar, M. Sotto, K. K. M. Grabska, D. Bajoni, M. Galli, S. Saito, and F. Y. F. Gardes, Ultrahigh-Q photonic crystal cavities in silicon rich nitride, *Opt. Express* **25**, 27334 (2017).
- [28] L.-D. Haret, T. Tanabe, E. Kuramochi, and M. Notomi, Extremely low power optical bistability in silicon demonstrated using 1D photonic crystal nanocavity, *Opt. Express* **17**, 21108 (2009).
- [29] V. R. Almeida and M. Lipson, Optical bistability on a silicon chip, *Opt. Lett.* **29**, 2387 (2004).
- [30] M. Notomi, A. Shinya, S. Mitsugi, G. Kira, E. Kuramochi, and T. Tanabe, Optical bistable switching action of Si high-Q photonic-crystal nanocavities, *Opt. Express* **13**, 2678 (2005).
- [31] T. Tanabe, K. Nishiguchi, A. Shinya, E. Kuramochi, H. Inokawa, M. Notomi, K. Yamada, T. Tsuchizawa, T. Watanabe, H. Fukuda, H. Shinojima, and S. Itabashi, Fast all-optical switching using ion-implanted silicon photonic crystal nanocavities, *Appl. Phys. Lett.* **90**, 031115 (2007).
- [32] G. Priem, P. Dumon, W. Bogaerts, D. Van Thourhout, G. Morthier, and R. Baets, Optical bistability and pulsating behaviour in silicon-on-insulator ring resonator structures, *Opt. Express* **13**, 9623 (2005).
- [33] W. H. P. Pernice, M. Li, and H. X. Tang, Time-domain measurement of optical transport in silicon micro-ring resonators, *Opt. Express* **18**, 18438 (2010).
- [34] V. Ilchenko and M. Gorodetsky, Thermal nonlinear effects in optical whispering gallery microresonators, *Laser Phys.* **2**, 1004 (1992).
- [35] S. Iadanza, M. Clementi, C. Hu, S. A. Schulz, D. Gerace, M. Galli, and L. O'Faolain, Model of thermo-optic nonlinear dynamics of photonic crystal cavities, *Phys. Rev. B* **102**, 245404 (2020).
- [36] R. Soref and B. Bennett, Electrooptical effects in silicon, *IEEE J. Quantum Electron.* **23**, 123 (1987).
- [37] We note that experimental results show that the Drude model is not sufficient to account for the whole phenomenology associated with FCD in some practical cases [36]. In particular, in the case of silicon the contribution to dispersion from electrons and holes is slightly different:

$$\frac{\Delta n}{n} = -\frac{1}{n}(\zeta_e N_e + \zeta_h N_h^{0.8})$$

- For simplicity, we will ignore this correction in the following discussion.
- [38] K. Nozaki, T. Tanabe, A. Shinya, S. Matsuo, T. Sato, H. Taniyama, and M. Notomi, Sub-femtojoule all-optical switching using a photonic-crystal nanocavity, *Nat. Photonics* **4**, 477 (2010).
 - [39] M. Belotti, M. Galli, D. Gerace, L. C. Andreani, G. Guizzetti, A. R. Md Zain, N. P. Johnson, M. Sorel, and R. M. De La Rue, All-optical switching in silicon-on-insulator photonic wire nano-cavities, *Opt. Express* **18**, 1450 (2010).
 - [40] T. Tanabe, M. Notomi, S. Mitsugi, A. Shinya, and E. Kuramochi, All-optical switches on a silicon chip realized using photonic crystal nanocavities, *Appl. Phys. Lett.* **87**, 151112 (2005).
 - [41] M. Waldow, T. Plötzing, M. Gottheil, M. Först, J. Bolten, T. Wahlbrink, and H. Kurz, 25ps all-optical switching in oxygen implanted silicon-on-insulator microring resonator, *Opt. Express* **16**, 7693 (2008).
 - [42] F. Morichetti, A. Melloni, C. Ferrari, and M. Martinelli, Error-free continuously-tunable delay at 10 Gbit/s in a reconfigurable on-chip delay-line, *Opt. Express* **16**, 8395 (2008).
 - [43] M. Notomi, Manipulating light with strongly modulated photonic crystals, *Rep. Prog. Phys.* **73**, 096501 (2010).
 - [44] R. M. Osgood, N. C. Panoiu, J. I. Dadap, X. Liu, X. Chen, I.-W. Hsieh, E. Dulkeith, W. M. J. Green, and Y. A. Vlasov, Engineering nonlinearities in nanoscale optical systems: Physics and applications in dispersion-engineered silicon nanophotonic wires, *Adv. Opt. Photon* **1**, 162 (2009).